Progress In Electromagnetics Research, PIER 40, 29–53, 2003

STRIPLINE TRANSITION TO RIDGE WAVEGUIDE BANDPASS FILTERS

M. A. El Sabbagh, H.-T. Hsu, and K. A. Zaki

University of Maryland
Electrical & Computer Engineering Department
College Park, MD 20742, USA

P. Pramanick and T. Dolan

K & L Microwave Incorporated
Salisbury, MD 21801, USA

Abstract—Full wave optimization is implemented to design a wide band transition from shielded stripline to ridge waveguide. A bandpass ridge waveguide filter, with input/output realized through tapped-in stripline is designed. Using rigorous mode matching technique the generalized scattering matrices of all the building blocks are obtained. Design procedure is described and examples are given to demonstrate the features of the tapped-in coupling structure. The tapped-in structure results in a considerable reduction of the filter's total length compared to the use of two transitions.

1. INTRODUCTION

In modern communication systems, there is a growing need for small size, light weight and compact high performance RF/microwave elements. Since large areas in the printed circuit boards of systems are usually occupied by passive components, integration of the passive components into multilayers substrates [1] is an efficient way to miniaturize the size and to increase the reliability of the RF/microwave systems. RF and microwave filters are very important passive components, among which, 3-D cavity filters usually offer lower loss characteristics compared to the planar circuits [2]. Ridge waveguide filters are characterized by large single mode broadband operation because the dominant mode cutoff frequency of the ridge waveguide is smaller than that of a rectangular waveguide with the same cross section. Ridge waveguide filters also have low loss, high spurious performance and compact size. The design of ridge waveguide filters suitable for multilayers applications can be found in [3–5]. Fig. 1(a) [5] shows the configuration of a typical ridge waveguide filter using single ridge waveguide resonators. The coupling between each two resonators is achieved through a section of evanescent mode rectangular waveguide, operating below the cutoff frequency of the dominant mode of the single ridge waveguide. This configuration of ridge waveguide filters yields compact filters with moderate to wide bandwidth and good spurious performance. Transitions from the single ridge waveguide at the input and the output to the stripline as shown in Fig. 1(b) [4] is needed to make the filter compatible with other components in multilayers packages. Very good results were obtained for filters designed according to the configuration in Fig. 1. However, the input/-output ridge waveguides to the 50Ω stripline transition involves long multisections of striplines, redundant ridges and evanescent sections at the input and the output increasing the filter's total length. In this paper, mode matching is applied to get the generalized scattering matrix of the stripline to ridge waveguide discontinuity. Full wave modeling and optimization of the transition from a 50Ω stripline to ridge waveguide is presented. Also, it is shown how to replace the input and output sections and transitions by direct tapped connections to the first and the last resonators as shown in Fig. 2(a). In the examples, the resulting total filter's length reduction is between 36% and

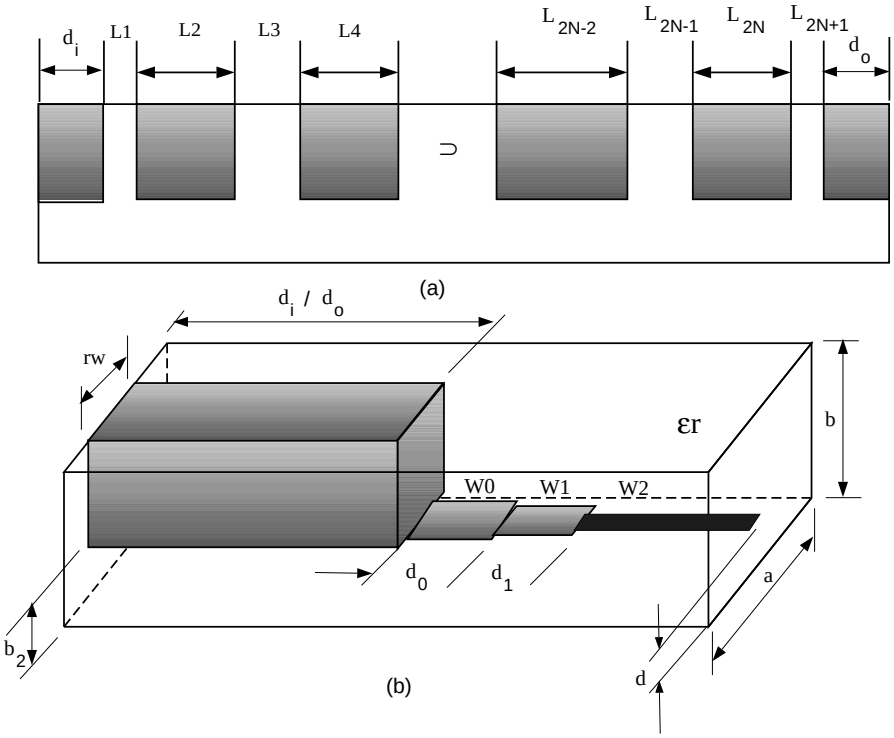

Figure 1. (a) Configuration of a N poles ridge waveguide filter. (b) Transition from single ridge waveguide to 50Ω stripline at the input and the output. Dimensions: $N = 5$, $a = 0.3$ in, $b = 0.096$ in, $b_2 = 0.012$ in, $d = 0.012$ in, $rw = 0.1$ in, $\epsilon_r = 3.38$, $d_i = d_o = 0.030$ in, $L_1 = 0.0837$ in, $L_2 = 0.1239$ in, $L_3 = 0.2123$ in, $L_4 = 0.0968$ in, $L_5 = 0.2576$ in, $L_6 = 0.0949$ in, $L_7 = L_5$, $L_8 = L_4$, $L_9 = L_3$, $L_{10} = L_2$, $L_{11} = L_1$, stripline thickness $= 0.0005$ in, $W_0 = 0.060$ in, $W_1 = 0.030$ in, $W_2 = 0.0215$ in, $d_0 = 0.115$ in, $d_1 = 0.145$ in.

70%. The full wave mode matching technique is used to obtain the generalized scattering matrices of all the building blocks. The building blocks are cascaded together to get the total filter's response. Full wave optimization is used to get the optimum filter's response.

2. MODELING

The filter shown in Fig. 2(a) is decomposed into building blocks characterized by their generalized scattering matrices. The building blocks

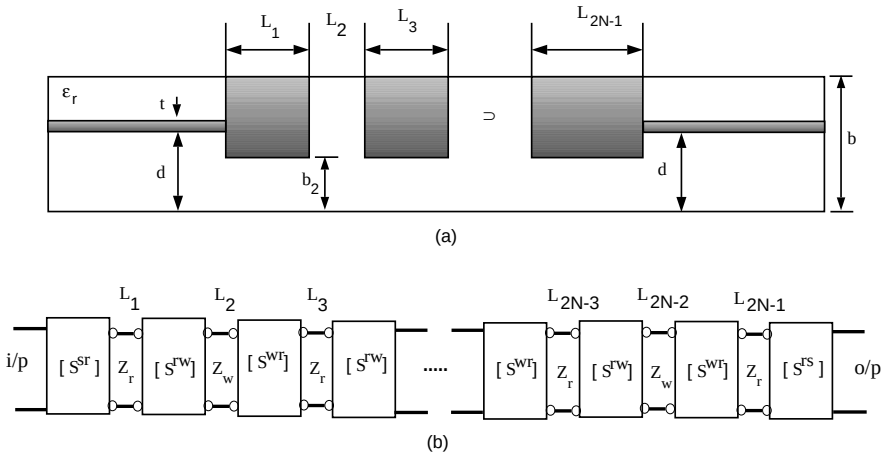

Figure 2. (a) Configuration of a N poles ridge waveguide filter excited by a tapped-in 50Ω stripline. Dimensions: $N = 5$, $a = 0.3$ in, $b = 0.096$ in, $b_2 = 0.012$ in, $d = 0.044$ in, $rw = 0.1$ in, $\epsilon_r = 3.38$, $t = 0.0005$ in, $L_1 = 0.1084$ in, $L_2 = 0.2027$ in, $L_3 = 0.0968$ in, $L_4 = 0.252$ in, $L_5 = 0.0953$ in, $L_6 = L_4$, $L_7 = L_3$, $L_8 = L_2$, $L_9 = L_1$, $W_0 = 0.0545$ in. (b) Generalized scattering matrices building blocks.

as shown in Fig. 2(b) are the discontinuity from the stripline to the ridge waveguide $[S^{sr}]$, the discontinuity from the ridge waveguide to the rectangular waveguide $[S^{rw}]$ and $[S^{wr}]$ is the discontinuity from the rectangular waveguide to the ridge waveguide. The filter shown in Fig. 1(a) requires the same building blocks in addition to the discontinuity from a stripline to a stripline $[S^{ss}]$. The generalized scattering matrices of these building blocks are obtained using the full wave mode matching technique. Before applying the mode matching, the eigenmodes in the stripline and in the ridge waveguide must be found.

2.1. Eigenmodes

The modes in the stripline are TEM, TE and TM modes, while, the modes in the ridge waveguide are TE and TM modes. For each of these modes, eigenfields within the guides are to be found first. The approach of getting the eigenmodes and their field distributions can be found in [2].

2.2. Generalized Scattering Matrix

After obtaining the eigenmodes and the corresponding field components, the mode matching technique is applied to obtain the generalized scattering matrices of all the discontinuities involved. At each side of a discontinuity, the fields are expressed as the superposition of the incident and the reflected waves of all the eigenmodes that are orthogonal and constitute a complete set of basis functions. By applying the boundary conditions at each discontinuity and performing appropriate inner products of these eigenmode fields, the generalized scattering matrices of the discontinuities are obtained. The discontinuity from ridge waveguide to empty waveguide is found in [8, 2]. The discontinuity from stripline to ridge waveguide is modeled next.

2.3. Stripline to Ridge Waveguide Discontinuity

The eigenmodes and their field distributions are used with a full wave modal analysis to characterize the discontinuity between the stripline and ridge waveguide (Fig. 3). The continuity of the tangential electric field at $z = 0$ gives:

$$\sum_{i=1}^{N_s} \left(a_i^s + b_i^s\right) \vec{e}_{ti}^{\,s} = \begin{cases} \sum_{i=1}^{N_r^h} \left(a_i^{rh} + b_i^{rh}\right) \vec{e}_{ti}^{\,rh} + \sum_{i=1}^{N_r^e} \left(a_i^{re} + b_i^{re}\right) \vec{e}_{ti}^{\,re} & b_3 < y < b_2 \\ 0 & \text{otherwise} \end{cases} \tag{1}$$

and the continuity of the tangential magnetic field gives:

$$\sum_{i=1}^{N_s} \left(a_i^s - b_i^s\right) \vec{h}_{ti}^{\,s} = \sum_{i=1}^{N_r^h} \left(-a_i^{rh} + b_i^{rh}\right) \vec{h}_{ti}^{\,rh} + \sum_{i=1}^{N_r^e} \left(-a_i^{re} + b_i^{re}\right) \vec{h}_{ti}^{\,re} \qquad b_3 < y < b_2 \tag{2}$$

where $(\vec{e}_{ti}^{\,s}, \vec{h}_{ti}^{\,s})$ are the tangential fields of the ith mode of the stripline, $(\vec{e}_{ti}^{\,rh}, \vec{h}_{ti}^{\,rh})$ and $(\vec{e}_{ti}^{\,re}, \vec{h}_{ti}^{\,re})$ are the tangential fields of ith TE and TM modes of the ridge waveguide respectively the z components of the fields are given in the appendix, N_s is the total number of modes (TEM, TE and TM) in the stripline, N_r^h, N_r^e number of TE and TM modes of the ridge waveguide respectively. Taking inner product to electric field continuity equation (1) with the magnetic field from the side with larger effective cross section (stripline) and taking inner product to the magnetic field continuity equation (2) with the electric field from

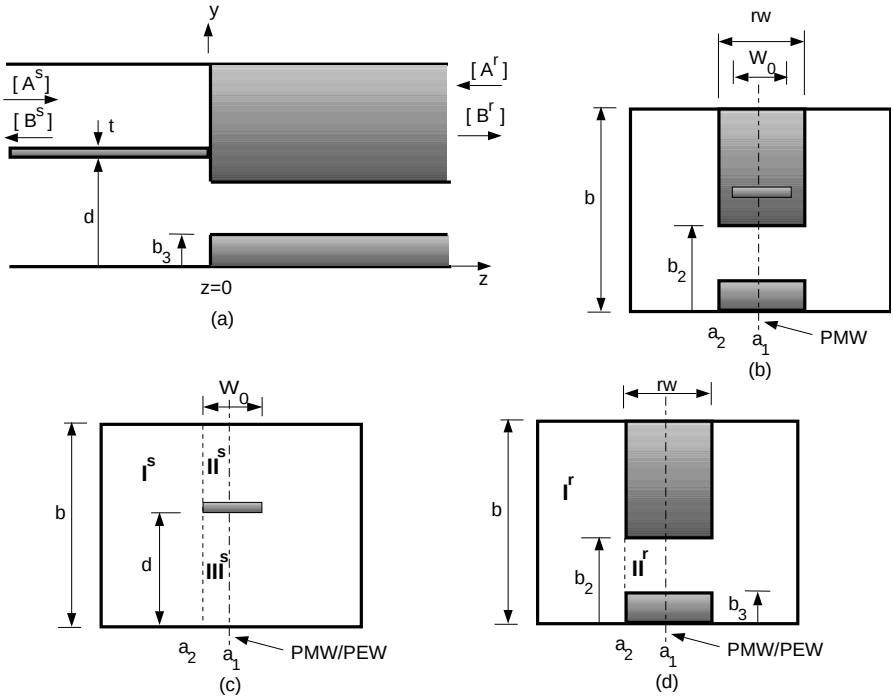

Figure 3. The configuration of a stripline to ridge waveguide discontinuity, (a) Side view, (b) Front view, (c) different regions in the cross section of a shielded stripline, (d) different regions in the cross section of a double ridge waveguide.

the side with smaller effective cross section (ridge waveguide) give the following:

$$[\lambda^s]\,(A^s + B^s) = [M]\,(A^r + B^r) \tag{3}$$

$$[M]^t\,(A^s - B^s) = [\lambda^r]\,(-A^r + B^r) \tag{4}$$

where $\lambda_i^{sp} = \langle \vec{e}_{ti}^{sp}, \vec{h}_{ti}^{sp} \rangle$, p = TEM,TE,TM, $\lambda_i^{rq} = \langle \vec{e}_{ti}^{rq}, \vec{h}_{ti}^{rq} \rangle$, q = TE,TM, t denotes the transpose of a matrix and the mutual inner product elements are defined as:

$$m_{ji} = \langle \vec{e}_{ti}^{rq}, j\omega\mu_o \vec{h}_{tj}^{sp} \rangle = \iint_{S_r} \left(\vec{e}_{ti}^{rq} \times j\omega\mu_o \vec{h}_{tj}^{sp} \right) \cdot d\vec{s} \tag{5}$$

From (3), (4), the generalized scattering matrix relating the incident and reflected coefficients is given by:

$$\begin{pmatrix} B^s \\ B^r \end{pmatrix} = \begin{pmatrix} [S_{11}^{sr}] & [S_{12}^{sr}] \\ [S_{21}^{sr}] & [S_{22}^{sr}] \end{pmatrix} \begin{pmatrix} A^s \\ A^r \end{pmatrix} = [S^{sr}] \begin{pmatrix} A^s \\ A^r \end{pmatrix} \tag{6}$$

with

$$\begin{aligned} [R] &= [\lambda^s]^{-1} [M] && (N_s \times N_r) \\ [T] &= [\lambda^r]^{-1} [M]^t && (N_r \times N_s) \\ [S_{11}^{sr}] &= ([R][T] + [U])^{-1} ([R][T] + [U]) && (N_s \times N_s) \\ [S_{12}^{sr}] &= 2([R][T] + [U])^{-1} [R] && (N_s \times N_r) \\ [S_{21}^{sr}] &= [T]([U] - [S_{11}^{sr}]) && (N_r \times N_s) \\ [S_{22}^{sr}] &= [U] - [T][S_{12}^{sr}] && (N_r \times N_r) \end{aligned} \tag{7}$$

where B^s and A^s are vectors of size N_s and their elements represent the reflected and incident coefficients of each mode at the stripline side, while B^r and A^r are vectors of size $N_r = N_r^h + N_r^e$ representing the reflected and incident mode coefficients at the ridge waveguide side, $[M]$ is the matrix of mutual inner products of size $N_s \times N_r$. $[S^{sr}]$ is the generalized S-matrix of the stripline to ridge waveguide discontinuity.

2.4. Stripline to Ridge Waveguide Transition

Transition from the input/output ridge waveguide to a 50Ω stripline are needed to make such filters, as shown in Fig. 1(a), compatible with other components in multilayer packages. The ridge waveguide and the stripline could have very similar field distributions. For the ridge waveguide, the field is concentrated under the ridge and for the stripline, the field is mainly concentrated beneath the center conductor. The transition from the ridge waveguide to the stripline must be designed such that more energy can flow smoothly from the ridge waveguide to the first section of the stripline. The two lines must have the same impedance at the center frequency of the filter, this gives the width of the stripline. A quarter-wave transformer is used to match the stripline connected directly to the ridge to the stripline with standard 50Ω impedance. Fig. 4(a), shows the configuration of two back to back transitions, each transition consists of N striplines sections. The generalized scattering matrices building blocks as shown in Fig. 4(b) are the discontinuity from stripline to stripline $[S^{ss}]$ and the discontinuity from stripline to the single ridge waveguide $[S^{sr}]$. The

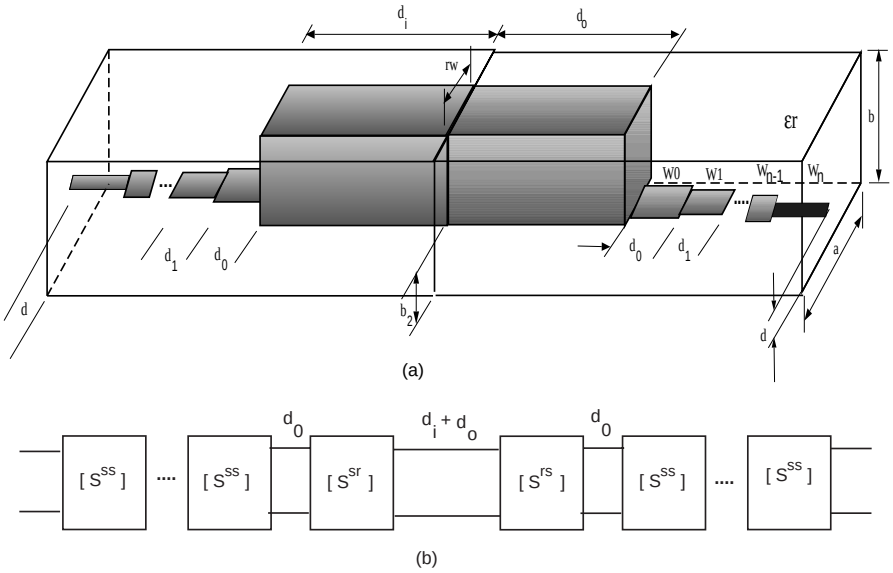

Figure 4. (a) The configuration of a back to back transition of 50Ω stripline to single ridge waveguide, (b) Generalized scattering matrices building blocks.

rigorous modal analysis is implemented to develop a software code to get an optimum design of stripline to ridge waveguide transition. The two back to back transition model used here, helps to test the quality of the transitions, and examine the effect of the input/output ridge length on the total response when a transition is used to match the filter. For example, when the filter of the configuration shown in Fig. 1(a) is placed between two transitions, the input/output ridge's length may degrade the return loss. It is required to consider this length as an optimization variable when the transition is connected to the filter.

2.5. Filter Design

The dimensions of the evanescent mode waveguide are determined so that its fundamental mode cutoff frequency is much higher than the filter operating center frequency. All, the ridge waveguides are chosen to have the same cutoff frequencies. The filter design consists of two steps. The first is the prototype synthesis to get the required impedance inverters [7, 8] for the inner sections of the filter and to realize the required input/output coupling. A modification factor [4] is introduced to modify the fractional bandwidth of the synthesized

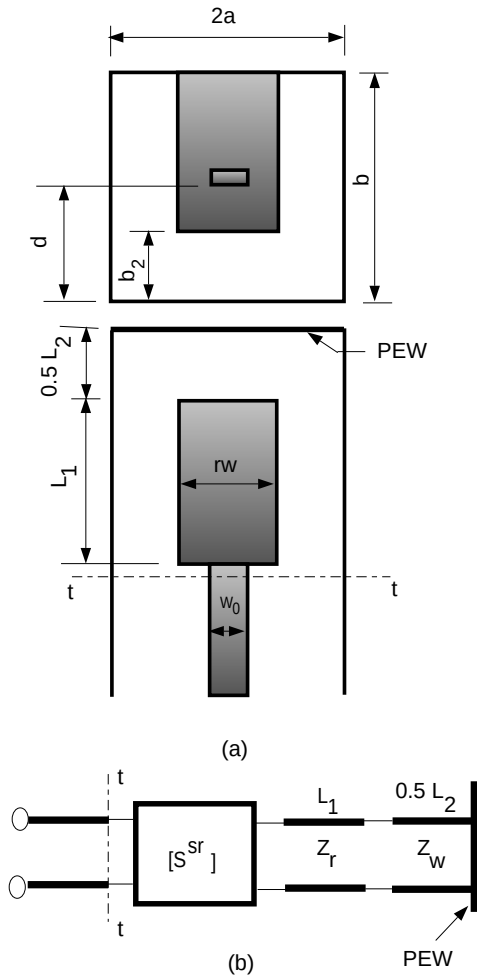

Figure 5. (a) The configuration used to compute the input/output coupling of a ridge waveguide filter excited by a tapped-in 50Ω stripline. (b) Generalized scattering matrices building blocks.

filter that turns out to be wider than the desired bandwidth due to dispersion effects and large bandwidth that are not considered in [7]. Fig. 5 shows the configuration and the corresponding building blocks used to compute the input/output coupling. For a single coupled resonator that has the equivalent circuit in [9] the coupling is related

to the frequency and the phase angle by the following equation:

$$\frac{d\phi}{d\omega} = \frac{2}{R} \frac{1}{1 + \left(\frac{\lambda}{R}\right)^2} \frac{\omega^2 + \omega_l^2}{\omega_l \omega^2} \tag{8}$$

where ϕ is the phase angle of the input reflection coefficient obtained at the reference plane $t-t$, ω_l is the loaded resonant frequency, $\lambda = \frac{\omega}{\omega_l} - \frac{\omega_l}{\omega}$ and R is the normalized (w.r.t. the resonator characteristic impedance) input/output coupling. R can be expressed as:

$$R = \left[-\frac{\omega^2 + \omega_l^2}{\omega_l \omega^2} \pm \sqrt{\frac{\omega^2 + \omega_l^2}{\omega_l \omega^2} - \left(\frac{\omega}{\omega_l} - \frac{\omega_l}{\omega}\right)} \right] / \frac{d\phi}{d\omega} \tag{9}$$

The slope $d\phi/d\omega$ is maximum when $\omega = \omega_l$ and this gives the following relation to get the coupling in terms of the maximum slope variation and the loaded resonant frequency:

$$R = -\frac{4}{f_l \frac{d\phi}{df}\Big|_{\max}} \tag{10}$$

The coupling bandwidth in MHz is defined as:

$$R\,(\text{MHz}) = R \times f_l\,(\text{MHz}) \tag{11}$$

The stripline dimensions are changed until the required coupling is achieved. The second step is the full wave optimization to get the optimum filter parameters. As described in [6,8], an objective function is defined and is minimized efficiently using a gradient optimization method together with a numerical interpolation technique.

3. NUMERICAL RESULTS

3.1. Stripline to Single Ridge Waveguide Discontinuity

A computer program was developed to calculate the generalized scattering matrix $[S^{sr}]$. Fig. 6, shows the convergence of the scattering parameters of the dominant mode on each side of the discontinuity from stripline (port 1) to a single ridge waveguide at 10.0 GHz. The number of basis functions is N_b and the number of modes in each side of the discontinuity is N ($N_s = N_r$). It was found that $N_b = 12$ and $N = 10$ are sufficient for convergence in most of the cases studied. Fig. 7 presents the S-parameters of the discontinuity between stripline and ridge waveguide. The results are in good agreement with those obtained from a commercial FEM software [10].

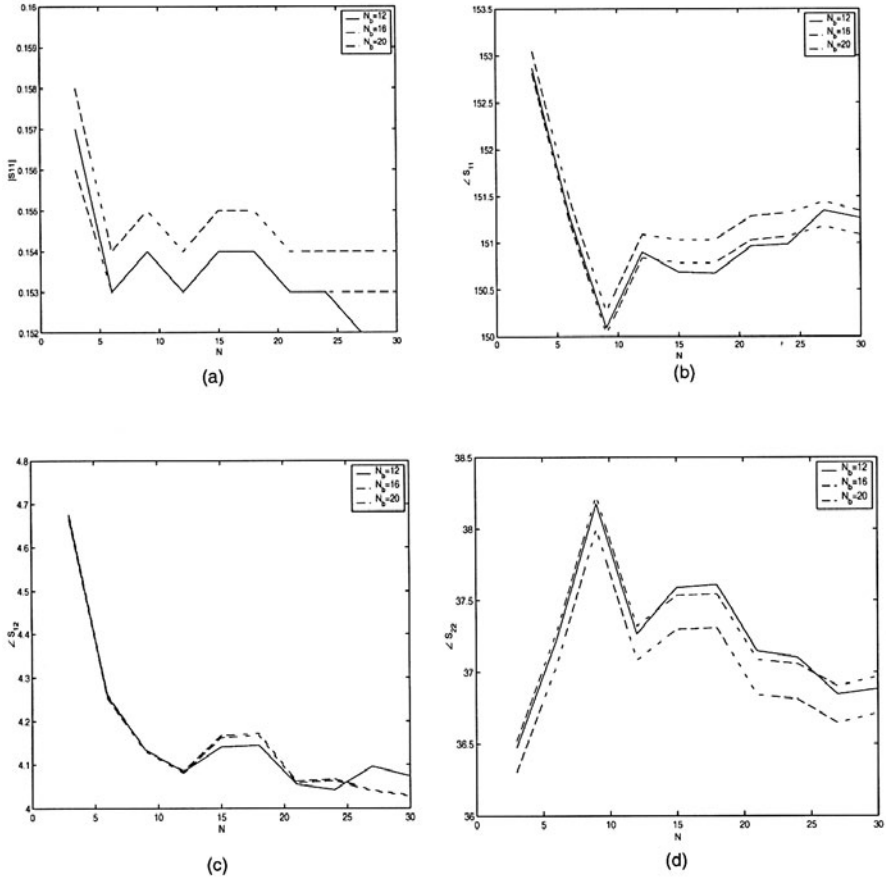

Figure 6. Convergence of the scattering parameters of the discontinuity from stripline to single ridge waveguide with N (number of modes) and N_b (number of basis functions), (a) $|S_{11}|$, (b) Phase S_{11}, (c) Phase S_{12}, (d) Phase S_{22}. Dimensions $a = 0.24\,\text{n}$, $b = 0.096\,\text{in}$, $rw = 0.08\,\text{in}$, $b_2 = d = 0.012\,\text{in}$, $\epsilon_r = 3.38$, $W_0 = 0.06\,\text{in}$, stripline thickness $= 0.0005\,\text{in}$.

3.2. Back to Back Transitions

Fig. 8 shows the return loss of a back to back transition as a function of frequency for different lengths of the input/output ridge (d_i/d_o). On the same graph, the return loss of the full wave optimized single transition is shown. The single transition has a good return loss over a very wide band. It is clear from this figure how the input/output ridge length affects the return loss. When the transition is connected

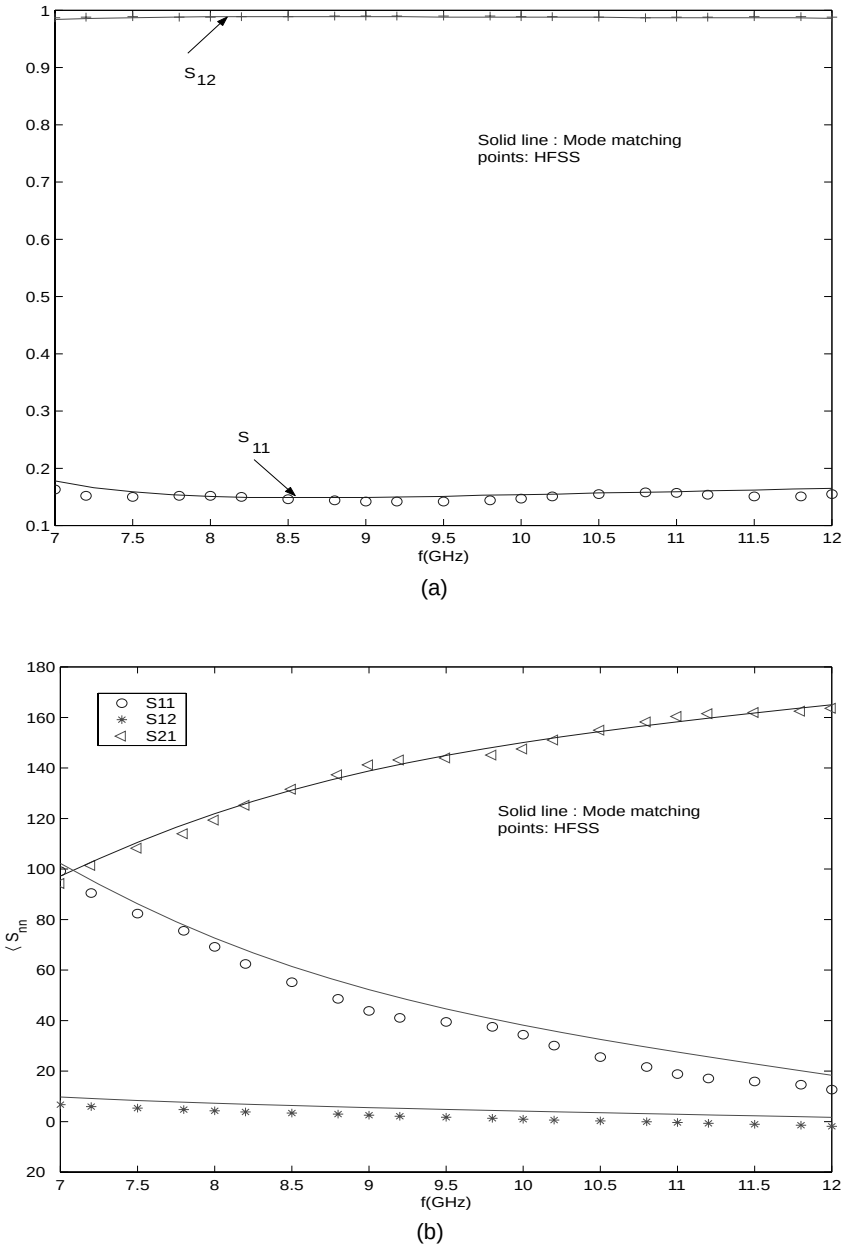

Figure 7. Scattering parameters of the discontinuity from stripline to single ridge waveguide, (a) Magnitude, (b) Phase. Dimensions same as in Fig. 6, number of TE modes = 6, of TM modes = 3, $N_b = 12$.

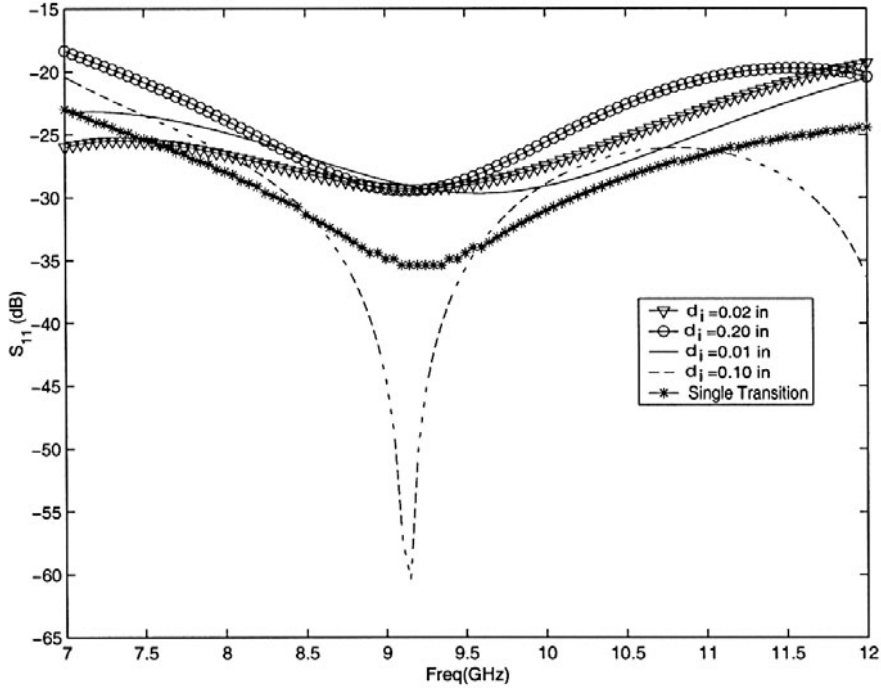

Figure 8. Effect of the input ridge length on the return loss of two back to back transitions. Number of stripline sections = 4, number of TE modes = 6, of TM modes = 3, $N_b = 12$. Dimensions as in Fig. 4: $a = 0.42\,\text{in}$, $b = 0.096\,\text{in}$, $b_2 = 0.012\,\text{in}$, $d = 0.012\,\text{in}$, $rw = 0.14\,\text{in}$, $\epsilon_r = 3.38$, stripline thickness $= 0.0005\,\text{in}$, $W_0 = 0.1\,\text{in}$, $W_1 = 0.06\,\text{in}$, $W_2 = 0.032\,\text{in}$, $W_3 = 0.0215\,\text{in}$, $d_0 = 0.277\,\text{in}$, $d_1 = 0.349\,\text{in}$, $d_2 = 0.298\,\text{in}$.

at the input and output of the filter shown in Fig. 1(a), it is necessary to include the input/output ridge's length as an optimization variable to get a good return loss in the passband.

3.3. Input/Output Coupling

In order to eliminate the transitions and reduce the overall filter length, the input/output coupling may be realized as a direct tapping of the stripline to the ridge waveguide. Fig. 9 shows the variation of the coupling in MHz and the loaded resonant frequency as a function of the tap-in position while the stripline width is held fixed. This curve shows that the coupling is a maximum (1860 MHz) when the stripline is

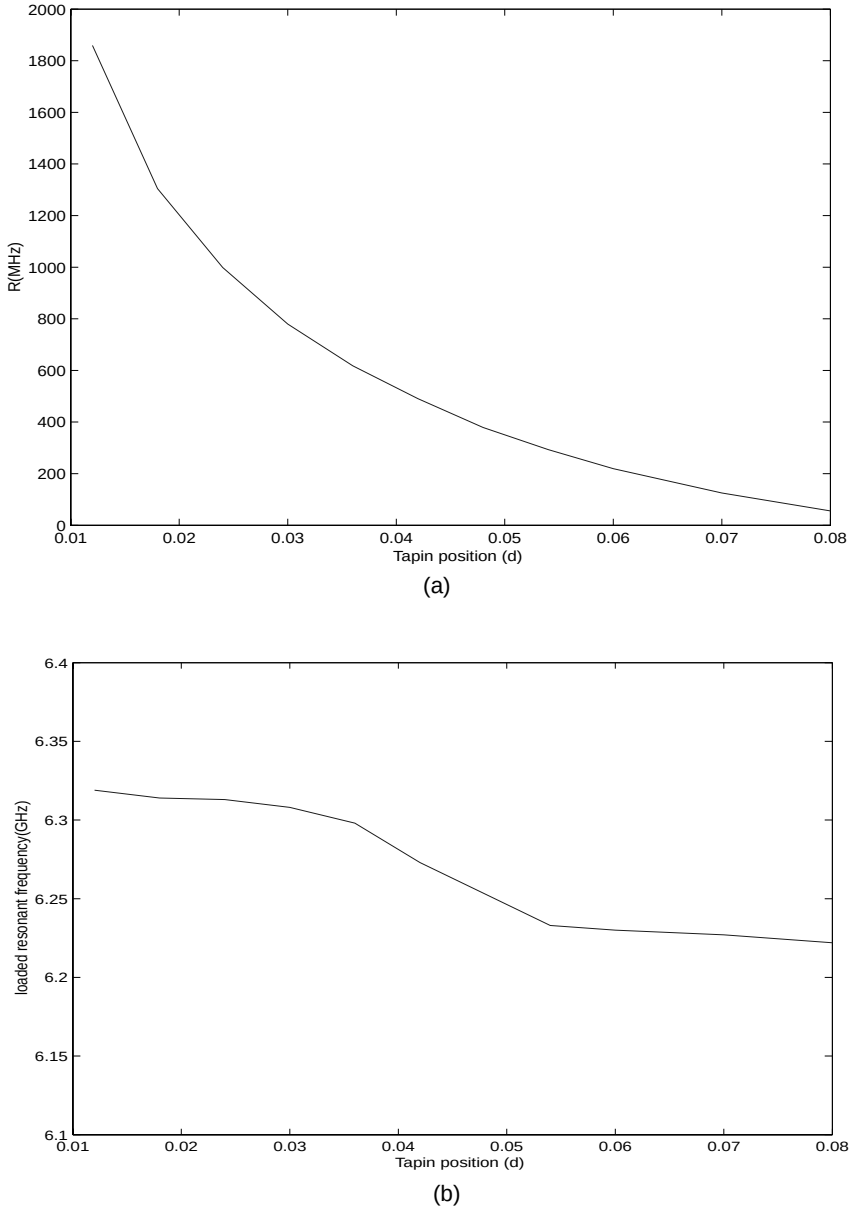

Figure 9. (a) The coupling in MHz as a function of the tap-in position, (b) The loaded resonant frequency as a function of the tap-in position. Dimensions as in Fig. 5: $2a = 0.3\,\text{in}$, $b = 0.096\,\text{in}$, $b_2 = 0.012\,\text{in}$, $rw = 0.1\,\text{in}$, $\epsilon_r = 3.38$, $W_0 = 0.0215\,\text{in}$, $L_1 = 0.123\,\text{in}$, $L_2 = 0.2\,\text{in}$.

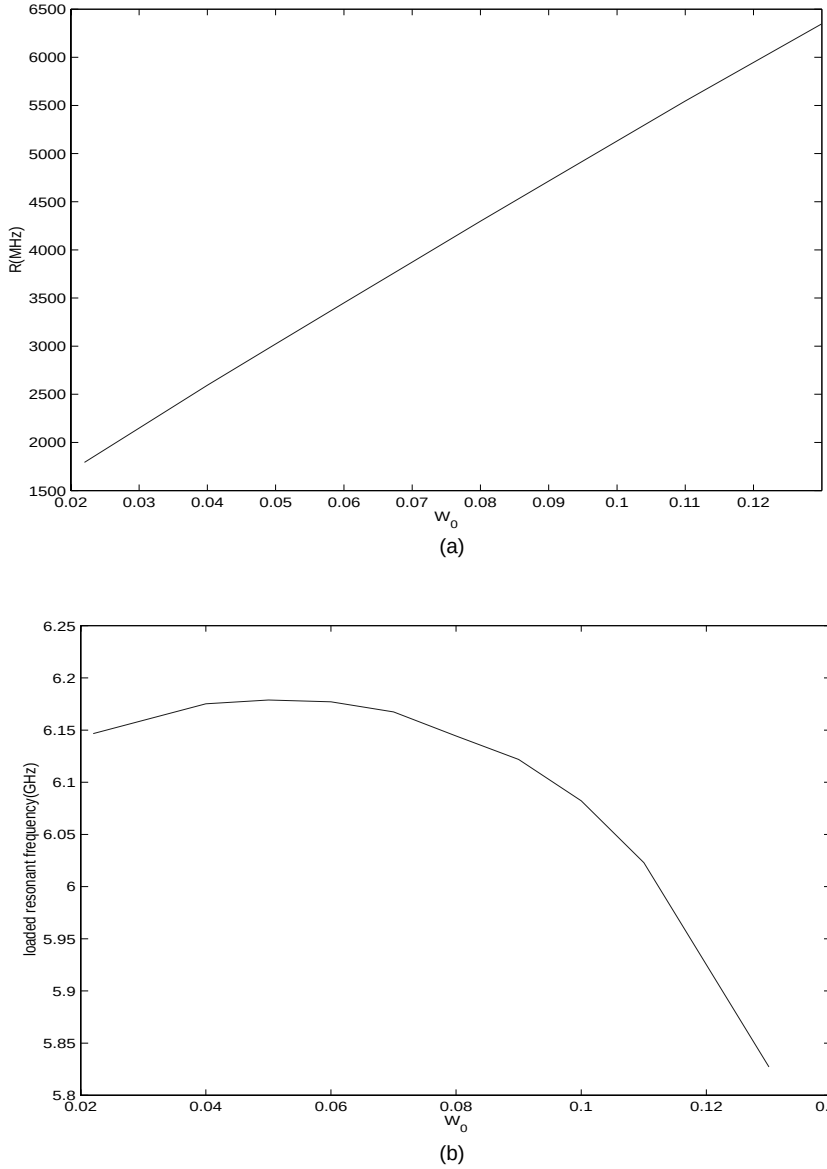

Figure 10. (a) The coupling in MHz and (b) The loaded resonant frequency as a function of the stripline width. Dimensions as in Fig. 5: $2a = 0.42\,\text{in}$, $b = 0.096\,\text{in}$, $b_2 = 0.012\,\text{in}$, $rw = 0.14\,\text{in}$, $d = 0.012\,\text{in}$, $\epsilon_r = 3.38$, $L_1 = 0.090\,\text{in}$, $L_2 = 0.1351\,\text{in}$.

tapped at the bottom of the ridge, as the stripline is shifted up toward the ground plane, the coupling is rapidly decreasing to a minimum (56 MHz). Correspondingly, the loaded resonant frequency goes down by 97 MHz. Fig. 10 shows the variation of the coupling in MHz and the loaded resonant frequency as a function of the stripline width while the tap-in position is held fixed. This curve shows that as the stripline width gets wider the coupling increases. While the loaded resonant frequency decreases. As the tap-in position or the stripline width is changed the stripline's characteristic impedance also changes. To keep the stripline's impedance at 50Ω and to achieve the required coupling simultaneously, it is required to optimize for both the tap-in position and stripline's width simultaneously.

3.4. Filter Design

Few filter design examples are presented to show the application of the tap-in stripline and its advantage in filter's length reduction. The first example compares two 5 poles ridge waveguide bandpass filters, one filter with transitions (Fig. 1) and the other with tapped-in (Fig. 2). Both filters have 6.175 GHz center frequency, 0.5 GHz bandwidth, and input coupling $R = 1.402761$. Fig. 11 shows a comparison of the in-band and the out-of-band frequency response of the two filters. The total length of the filter with input/output transitions is 2223.5 mils and the tapped-in filter has a total length of 1415.1 mils (reduction of 36.5% in length). A second example compares two 5 poles ridge waveguide bandpass filters, both have 6.175 GHz center frequency and 1.8 GHz bandwidth. Fig. 12 shows a comparison of the in-band and the out-of-band frequency response of the two filters. The filter with input/output transitions has a total length of 3038.1 mils and the tapped-in filter has a total length of 928.3 mils (a 70% reduction in length from the conventional filter). Another interesting application of the same topic is the interdigital bandpass filters. From the analysis point of view, interdigital filters can be modeled exactly the same way as double-ridge waveguide filters. This concept can be well illustrated in Fig. 13, where the cross sections (transverse to the direction of propagation) of the interdigital filters are related to that of double-ridge waveguide filters. To demonstrate the feasibility of this concept, an 8-pole interdigital filter with center frequency 2.14 GHz and 152 MHz bandwidth is designed and manufactured. The input and output of the filter are realized using tapped-in lines [11, 12]. The detailed dimensions are shown in Fig. 14. The simulated response using rigorous mode matching technique is included in Fig. 15. Fig. 16 shows the experimental results which is in good agreement with the simulated response.

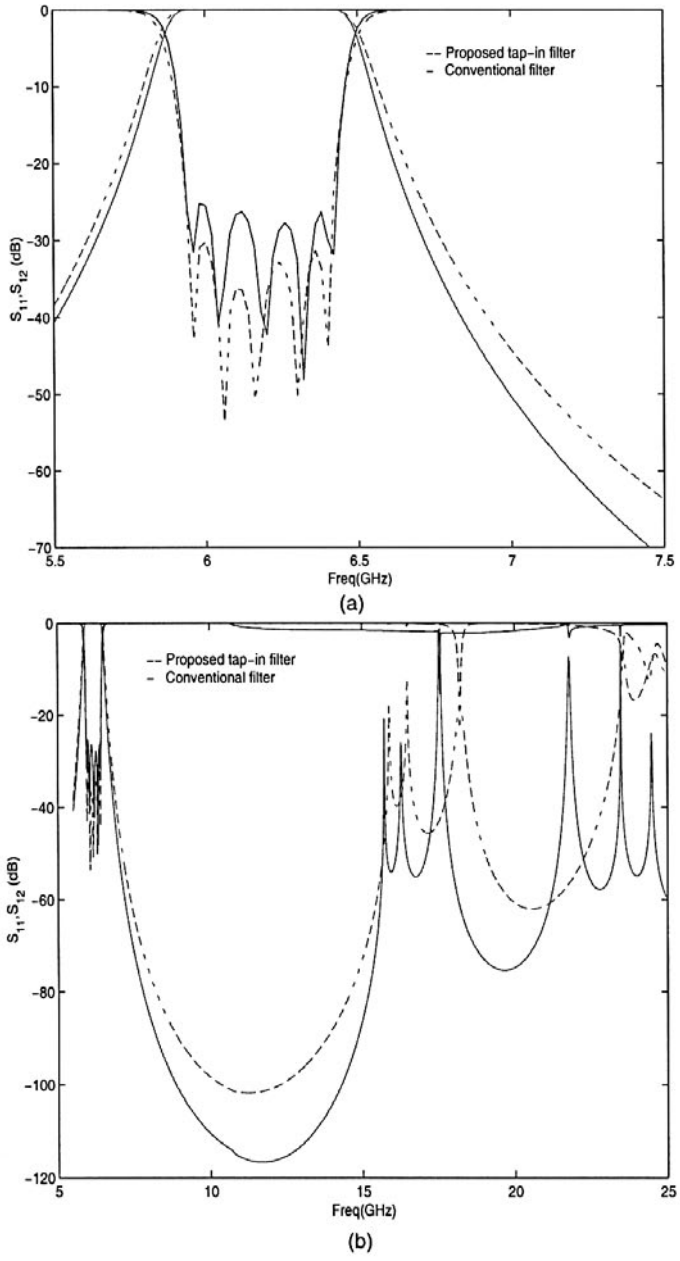

Figure 11. Comparison of frequency response of the filters shown in Figs. 1, 2 (a) In-band (b) Out-of-band. Dimensions same as in Figs. 1, 2.

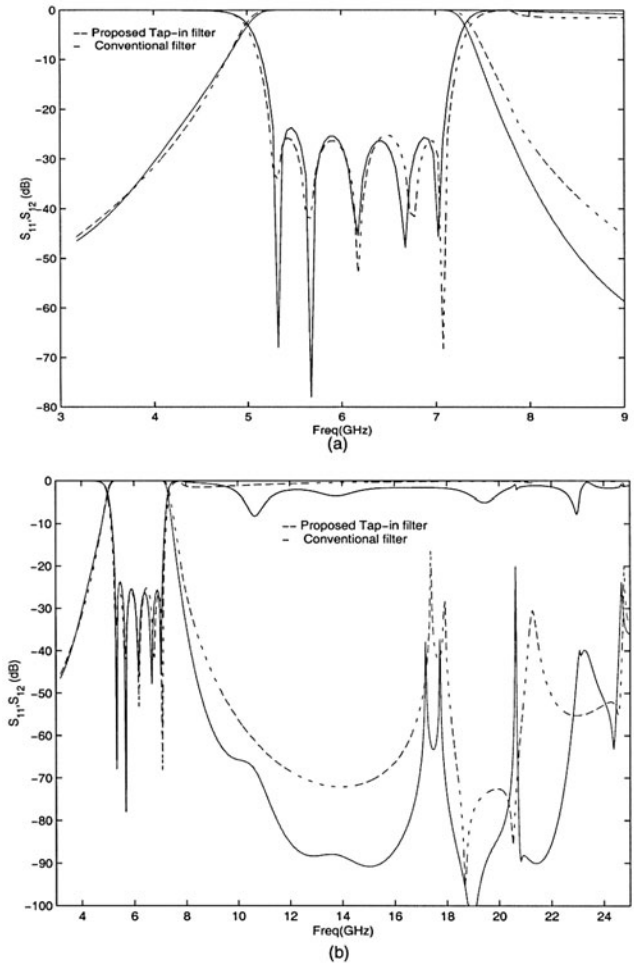

Figure 12. Comparison of frequency response of the filters shown in Figs. 1, 2 (a) In-band (b) Out-of-band. Dimensions used are: $N = 5$, $a = 0.42$ in, $b = 0.096$ in, $b_2 = 0.012$ in, $d = 0.012$ in, $rw = 0.14$ in, $\epsilon_r = 3.38$, Filter's in Fig. 1 dimensions: $d_i = d_o = 0.030$ in, $L_1 = 0.0379$ in, $L_2 = 0.1163$ in, $L_3 = 0.1314$ in, $L_4 = 0.0576$ in, $L_5 = 0.1984$ in, $L_6 = 0.0469$ in, $L_7 = 0.1984$ in, $L_8 = 0.0576$ in, $L_9 = 0.1314$ in, $L_{10} = 0.1163$ in, $L_{11} = 0.0379$ in, stripline thickness $= 0.0005$ in, $W_0 = 0.1$ in, $W_1 = 0.06$ in, $W_2 = 0.032$ in, $W_3 = 0.0215$ in, $d_0 = 0.277$ in, $d_1 = 0.349$ in, $d_2 = 0.298$ in. Filter's in Fig. 2 dimensions: $L_1 = 0.0552$ in, $L_2 = 0.1379$ in, $L_3 = 0.0521$ in, $L_4 = 0.196$ in, $L_5 = 0.0459$ in, $L_6 = 0.196$ in, $L_7 = 0.0521$ in, $L_8 = 0.1379$ in, $L_9 = 0.0552$ in, $W_0 = 0.022$ in.

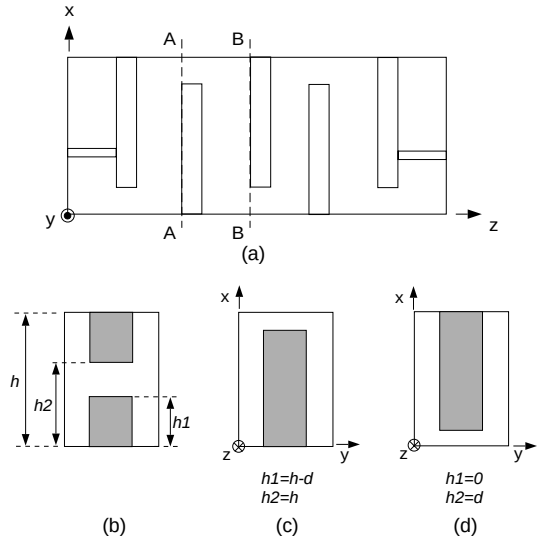

Figure 13. (a) Top view of a general interdigital bandpass filter; cross sectional views of (b) general double-ridge waveguide bandpass filter, (c) plane AA' and (d) plane BB' of the interdigital filter showing the relationship in the analysis point of view.

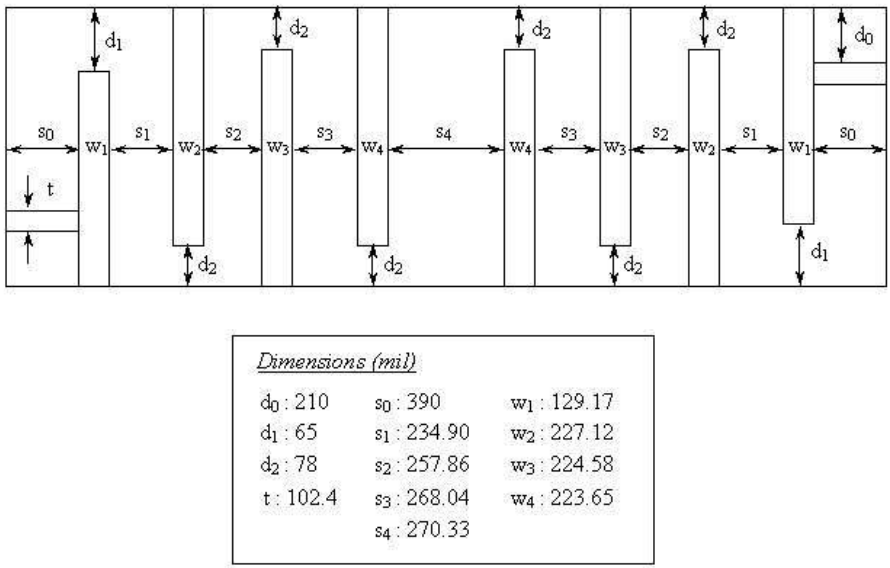

Figure 14. Configuration and dimensions of the tapped-in interdigital 8 poles filter.

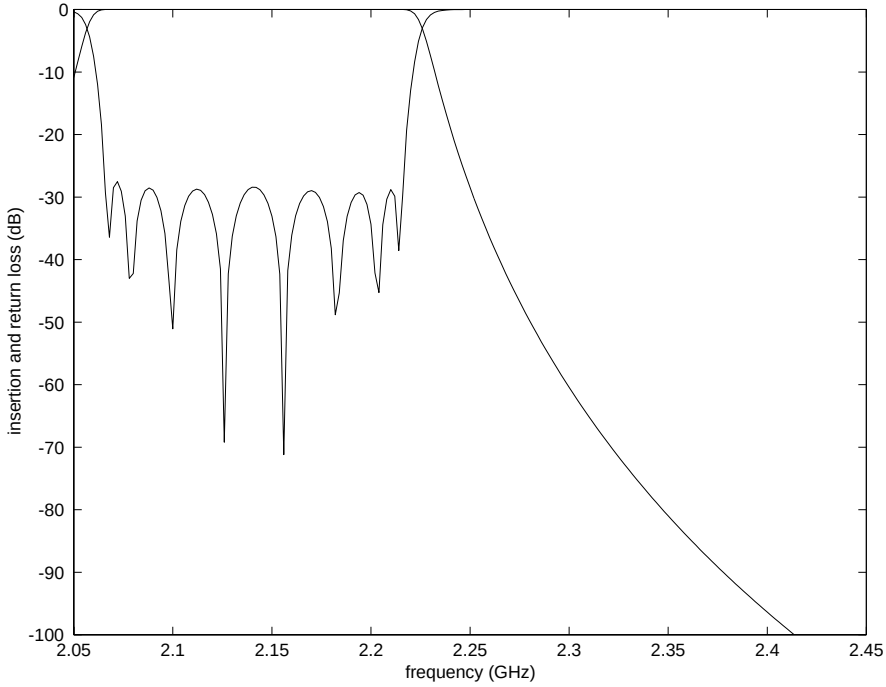

Figure 15. Simulation results using mode matching for the filter configuration shown in Fig. 14.

4. CONCLUSION

Full wave analysis is applied to model the discontinuity between a shielded stripline to a ridge waveguide. Numerical results for the convergence, and scattering parameters of the discontinuity are presented. Full wave optimization is used to design transitions from a 50Ω stripline to ridge waveguide.

A bandpass ridge waveguide filter with 50Ω tapped-in stripline is proposed for multilayers compact package. The mode matching technique is used to obtain the generalized scattering matrices of all the building blocks of the tapped-in ridge waveguide filter. Full wave optimization follows to get the optimum filter parameters. It is shown that the tapped-in ridge waveguide filter results in a significant length reduction compared to the conventional filter with input/output transitions. The accuracy of the numerical results are checked by comparison with HFSS and experimental data.

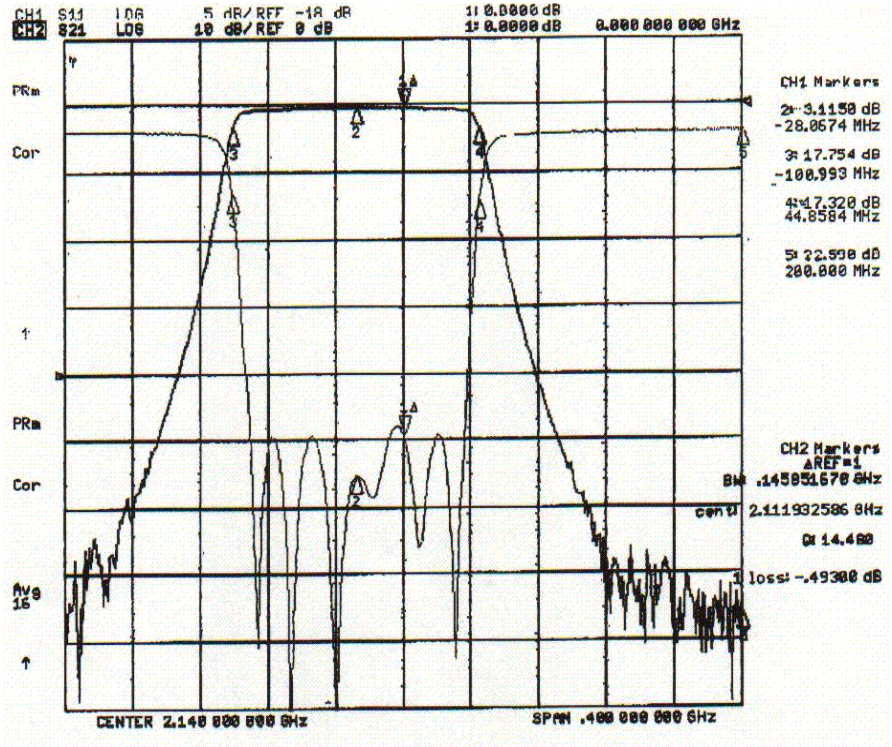

Figure 16. Experimental results for the filter configuration shown in Fig. 14.

APPENDIX A.

For the stripline, the scalar potential of the TEM mode, the z components of the magnetic field (for TE mode) and the electric field (for TM mode) in each region in Fig. 3(c) are given as follows:
For TEM mode:

$$\Phi^{Is} = \sum_{i=1}^{N_b} A_i^{\phi s} \sin k_{y1i}^{\phi s} y \frac{\sinh\left(k_{y1i}^{\phi s} x\right)}{\sinh\left(k_{y1i}^{\phi s} a_2\right)} \tag{A1}$$

$$k_{y1i}^{\phi s} = \frac{(i-1)\,\pi}{b}; \quad i = 1, 2, \ldots, N_b \tag{A2}$$

$$\Phi^{II^s} = \phi_o \frac{b-y}{b-d-t} + \sum_{i=1}^{N_{b2}} B_i^{\phi s} \sin k_{y_{2i}}^{\phi s} (y-d-t) \frac{\cosh k_{y_{2i}}^{\phi s} (x-a_1)}{\cosh k_{y_{2i}}^{\phi s} (a_2-a_1)} \tag{A3}$$

$$k_{y_{2i}}^{\phi s} = \frac{(i-1)\pi}{b-d-t}; \quad i = 1, 2, \ldots, N_{b2} \tag{A4}$$

$$\Phi^{III^s} = \phi_o \frac{y}{d} + \sum_{i=1}^{N_{b3}} C_i^{\phi s} \sin k_{y_{3i}}^{\phi s} y \frac{\cosh k_{y_{3i}}^{\phi s} (x-a_1)}{\cosh k_{y_{3i}}^{\phi s} (a_2-a_1)} \tag{A5}$$

$$k_{y_{3i}}^{\phi s} = \frac{(i-1)\pi}{d}; \quad i = 1, 2, \ldots, N_{b3} \tag{A6}$$

For TE mode:

$$j\omega\mu_o H_z^{I^s h} = \sum_{i=1}^{N_b} A_i^{hs} \cos k_{y_{1i}}^{hs} y \frac{\cosh k_{x_{1i}}^{hs} x}{\cosh k_{x_{1i}}^{hs} a_2} \tag{A7}$$

$$k_{y_{1i}}^{hs} = \frac{(i-1)\pi}{b}; \quad i = 1, 2, \ldots, N_b \tag{A8}$$

$$\left(k_{x_{1i}}^{hs}\right)^2 = \left(k_{y_{1i}}^{hs}\right)^2 - \left(k_c^{hs}\right)^2 \tag{A9}$$

$$j\omega\mu_o H_z^{II^s h} = \sum_{i=1}^{N_{b2}} B_i^{hs} \cos k_{y_{2i}}^{hs} (y-d-t) \begin{cases} \dfrac{\sinh k_{x_{2i}}^{hs} (x-a_1)}{\sinh k_{x_{2i}}^{hs} (a_2-a_1)} & \text{PMW} \\ \dfrac{\cosh k_{x_{2i}}^{hs} (x-a_1)}{\cosh k_{x_{2i}}^{hs} (a_2-a_1)} & \text{PEW} \end{cases} \tag{A10}$$

$$k_{y_{2i}}^{hs} = \frac{(i-1)\pi}{b-d-t}; \quad i = 1, 2, \ldots, N_{b2} \tag{A11}$$

$$\left(k_{x_{2i}}^{hs}\right)^2 = \left(k_{y_{2i}}^{hs}\right)^2 - \left(k_c^{hs}\right)^2 \tag{A12}$$

$$j\omega\mu_o H_z^{III^s h} = \sum_{i=1}^{N_{b3}} C_i^{hs} \cos k_{y_{3i}}^{hs} y \begin{cases} \dfrac{\sinh k_{x_{3i}}^{hs} (x-a_1)}{\sinh k_{x_{3i}}^{hs} (a_2-a_1)} & \text{PMW} \\ \dfrac{\cosh k_{x_{3i}}^{hs} (x-a_1)}{\cosh k_{x_{3i}}^{hs} (a_2-a_1)} & \text{PEW} \end{cases} \tag{A13}$$

$$k_{y_{3i}}^{hs} = \frac{(i-1)\pi}{d}; \quad i = 1, 2, \ldots, N_{b3} \tag{A14}$$

$$\left(k_{x_{3i}}^{hs}\right)^2 = \left(k_{y_{3i}}^{hs}\right)^2 - \left(k_c^{hs}\right)^2 \tag{A15}$$

For TM mode:

$$E_z^{I^s e} = \sum_{i=1}^{N_b} A_i^{es} \sin k_{y_{1i}}^{es} y \frac{\sinh k_{x_{1i}}^{es} x}{\sinh k_{x_{1i}}^{es} a_2} \tag{A16}$$

$$k_{y_{1i}}^{es} = \frac{i\pi}{b}; \quad i = 1, 2, \ldots, N_b \tag{A17}$$

$$\left(k_{x_{1i}}^{es}\right)^2 = \left(k_{y_{1i}}^{es}\right)^2 - \left(k_c^{es}\right)^2 \tag{A18}$$

$$E_z^{II^s e} = \sum_{i=1}^{N_{b2}} B_i^{es} \sin k_{y_{2i}}^{es} (y - d - t) \begin{cases} \dfrac{\cosh k_{x_{2i}}^{es} (x - a_1)}{\cosh k_{x_{2i}}^{es} (a_2 - a_1)} & \text{PMW} \\ \dfrac{\sinh k_{x_{2i}}^{es} (x - a_1)}{\sinh k_{x_{2i}}^{es} (a_2 - a_1)} & \text{PEW} \end{cases} \tag{A19}$$

$$k_{y_{2i}}^{es} = \frac{i\pi}{b - d - t}; \quad i = 1, 2, \ldots, N_{b2} \tag{A20}$$

$$\left(k_{x_{2i}}^{es}\right)^2 = \left(k_{y_{2i}}^{es}\right)^2 - \left(k_c^{es}\right)^2 \tag{A21}$$

$$E_z^{III^s e} = \sum_{i=1}^{N_{b3}} C_i^{es} \sin k_{y_{3i}}^{es} y \begin{cases} \dfrac{\cosh k_{x_{3i}}^{es} (x - a_1)}{\cosh k_{x_{3i}}^{es} (a_2 - a_1)} & \text{PMW} \\ \dfrac{\sinh k_{x_{3i}}^{es} (x - a_1)}{\sinh k_{x_{3i}}^{es} (a_2 - a_1)} & \text{PEW} \end{cases} \tag{A22}$$

$$k_{y_{3i}}^{es} = \frac{i\pi}{d}; \quad i = 1, 2, \ldots, N_{b3} \tag{A23}$$

$$\left(k_{x_{3i}}^{es}\right)^2 = \left(k_{y_{3i}}^{es}\right)^2 - \left(k_c^{es}\right)^2 \tag{A24}$$

where the superscripts ϕ, h, e denote TEM, TE, TM modes respectively. N_b, N_{b2}, N_{b3} denote the number of basis functions used in regions I, II, III respectively. For the ridge waveguide, the z components of the magnetic field (for TE mode) and the electric field (for TM mode) in each region in Fig. 3(d) are given as follows:
For TE mode:

$$j\omega\mu_o H_z^{I^r h} = \sum_{i=1}^{N_b} A_i^{hr} \cos k_{y_{1i}}^{hr} y \cosh k_{x_{1i}}^{hr} x \tag{A25}$$

$$k_{y_{1i}}^{hr} = \frac{(i-1)\,\pi}{b}; \quad i = 1, 2, \ldots, N_b \tag{A26}$$

$$\left(k_{x_{1i}}^{hr}\right)^2 = \left(k_{y_{1i}}^{hr}\right)^2 - \left(k_c^{hr}\right)^2 \tag{A27}$$

$$j\omega\mu_o H_z^{II^r h} = \sum_{i=1}^{N_{b2}} B_i^{hr} \cos k_{y_{2i}}^{hr} (y - b_2) \begin{cases} \dfrac{\sinh k_{x_{2i}}^{hr} (x - a_1)}{k_{x_{2i}}^{hr}} & \text{PMW} \\ \cosh k_{x_{2i}}^{hr} (x - a_1) & \text{PEW} \end{cases} \tag{A28}$$

$$k_{y_{2i}}^{hr} = \frac{(i-1)\,\pi}{b_2 - b_3}; \quad i = 1, 2, \ldots, N_{b2} \tag{A29}$$

$$\left(k_{x_{2i}}^{hr}\right)^2 = \left(k_{y_{2i}}^{hr}\right)^2 - \left(k_c^{hr}\right)^2 \tag{A30}$$

For TM mode:

$$E_z^{I^r e} = \sum_{i=1}^{N_b} A_i^{er} \sin k_{y_{1i}}^{er} y \frac{\sinh k_{x_{1i}}^{er} x}{k_{x_{1i}}^{er}} \tag{A31}$$

$$k_{y_{1i}}^{er} = \frac{i\pi}{b}; \quad i = 1, 2, \ldots, N_b \tag{A32}$$

$$\left(k_{x_{1i}}^{er}\right)^2 = \left(k_{y_{1i}}^{er}\right)^2 - (k_c^{er})^2 \tag{A33}$$

$$E_z^{II^r e} = \sum_{i=1}^{N_{b2}} B_i^{er} \sin k_{y_{2i}}^{er} (y - b_2) \begin{cases} \cosh k_{x_{2i}}^{er} (x - a_1) & \text{PMW} \\ \dfrac{\sinh k_{x_{2i}}^{er} (x - a_1)}{k_{x_{2i}}^{er}} & \text{PEW} \end{cases} \tag{A34}$$

$$k_{y_{2i}}^{er} = \frac{i\pi}{b_2 - b_3}; \quad i = 1, 2, \ldots, N_{b2} \tag{A35}$$

$$\left(k_{x_{2i}}^{er}\right)^2 = \left(k_{y_{2i}}^{er}\right)^2 - (k_c^{er})^2 \tag{A36}$$

REFERENCES

1. Bailey, A., W. Foley, M. Hageman, C. Murray, A. Piloto, K. Sparks, and K. Zaki, "Miniature LTCC filters for digital receivers," *1997 IEEE MTT-S Int. Microwave Symp. Digest*, 999–1002, 1997.
2. Wang, C. and K. A. Zaki, "Full-wave modeling of generalized double ridge waveguides T-junctions," *IEEE Trans. Microwave Theory and Tech.*, Vol. 44, 2536–2542, Dec. 1996.
3. Gipprich, J., D. Stevens, M. Hageman, A. Piloto, K. Zaki, and Y. Rong, "Embedded waveguide filters for microwave and wireless applications using cofired ceramic technologies," *Proc. Int. Microelectron. Symp.*, 23–26, San Diego, CA, Nov. 1998.

4. Rong, Y., K. Zaki, M. Hageman, D. Stevens, and J. Gipprich, "Low temperature cofired ceramic (LTCC) ridge waveguide bandpass filters," *1999 IEEE MTT-S Int. Microwave Symp. Digest*, 1147–1150, 1999.
5. Rong, Y., K. Zaki, J. Gipprich, M. Hageman, and D. Stevens, "LTCC wide-band ridge-waveguide bandpass filters," *IEEE Trans. Microwave Theory Tech.*, Vol. MTT-47, No. 9, 1836–1840, Sept. 1999.
6. Yao, H.-W., A. E. Abdelmonem, J. F. Liang, and K. A. Zaki, "Analysis and design of microstrip-to-waveguide transitions," *IEEE Trans. on Microwave Theory and Tech.*, Vol. 42, 2371–2380, Dec. 1994.
7. Matthaei, G., L. Young, and E. M. T. Jones, *Microwave Filters, Impedance-Matching Networks, and Coupling Structures*, Artech House, Norwood, MA, 1980.
8. Yao, H. W., A. E. Abdelmonem, J. F. Liang, X. P. Liang, and K. A. Zaki, "Wide-band waveguide and ridge waveguide T-junctions for diplexer applications," *IEEE Trans. Microwave Theory Tech.*, Vol. MTT-41, No. 12, 2166–2173, Dec. 1993.
9. Wang, C. and K. A. Zaki, "Modeling of couplings between double-ridge waveguide and dielectric-loaded resonator," *IEEE Trans. Microwave Theory Tech.*, Vol. MTT-46, No. 12, 2404–2411, Dec. 1998.
10. Agilent EEsof EDA, Palo Alto, CA, "Agilent high frequency structure simulator 5.5," December 1999.
11. Cristal, E. G., "Tapped-line coupling transmission lines with applications to interdigital and combline filters," *IEEE Trans. on Microwave Theory and Tech.*, Vol. MTT-23, 1007–1012, Dec. 1975.
12. Caspi, S. and J. Adelman, "Design of combling and interdigital filters with tapped-line input," *IEEE Trans. on Microwave Theory and Tech.*, Vol. 36, 759–763, Apr. 1988.